https://doi.org/10.1016/j.conbuildmat.2022.129836


# Bond behavior of CFRP-to-steel bonded joints at different service temperatures: Experimental study and FE modeling

Dong Guo[a], Yun-Lin Liu[b,c], Wan-Yang Gao[d,e*], Jian-Guo Dai[a*]

[a] Department of Civil and Environmental Engineering, The Hong Kong Polytechnic University, Hong Kong 999077, China.

[b] School of Civil Engineering, Anhui Jianzhu University, Hefei 230031, China.

[c] Prefabricated Building Research Institute of Anhui Province, Hefei 230031, China.

[d] Shanghai Key Laboratory for Digital Maintenance of Buildings and Infrastructure, School of Naval Architecture, Ocean and Civil Engineering, Shanghai Jiao Tong University, Shanghai 200240, China.

[e] State Key Laboratory of Ocean Engineering, Shanghai Jiao Tong University, Shanghai 200240, China.

*Corresponding authors: wanyanggao@sjtu.edu.cn (W.-Y. Gao), cejgdai@polyu.edu.hk (J.-G. Dai)

**Abstract:** The bond behavior of carbon fiber-reinforced polymer (CFRP)-to-steel interface in strengthened steel structures is likely to be significantly affected by service temperature variations, mainly because of interfacial thermal stresses and the changes in the local bond-slip behavior. However, there is lack of comprehensive study on the temperature effects on the bond behavior and the debonding load of the CFRP-to-steel interface at different service temperatures. This paper presents the results from the pull-out tests on CFRP-to-steel double-lap bonded joints tested at service temperatures ranging from -20 °C to 60 °C. The test results including failure modes, debonding loads, load-displacement curves, CFRP strain distributions and interfacial shear stress and slip responses are investigated and compared. Also, a bilinear local bond-slip model is developed to describe the relationships between the shear stresses and the interfacial slips at different service temperatures. A finite element (FE) model is proposed to predict the bond behavior and the debonding loads of the bonded joints at different service temperatures and validated through the comparisons between experimental and FE results. The validated FE model is then used to further investigate the temperature effects on the CFRP strain distributions, interfacial shear stresses and the debonding loads of the bonded joints at different service temperatures. The experimental and FE results have indicated that the debonding loads of the CFRP-to-steel interface are significantly reduced at both low and high service temperatures. The elastic stiffness and the peak shear stress of the local bond-slip model are generally reduced with the service temperature increase, while the interfacial fracture energy decreases at both low and high service temperatures.

**Keywords:** Carbon fiber-reinforced polymer (CFRP), steel, service temperature variations, thermal stress effect, double-lap bonded joints, interfacial debonding.

## 1. Introduction

Externally bonded (EB) carbon fiber-reinforced polymer (CFRP) composites are widely used to strengthen and retrofit steel structures using wet layup techniques. The composite action between EB CFRP plates and steel substrates is significantly dependent on their bond behavior. Since the strengths of the adherends (steel and CFRP) are much higher than that of the bonding adhesive, the failure of the strengthening system always occurs at the bond interface, which is referred to as debonding failure [1-3]. Therefore, the structural behaviors of EB CFRP-strengthened steel structures depend on the mechanical properties of the adhesives used to bond the CFRP plates to the existing steel structures.

Another key issue of CFRP-strengthened steel structures is their durability and resistance to harsh environments. Among the environmental factors that may adversely affect the behaviors of CFRP-strengthened steel structures, temperature effects should be appropriately considered during the strengthening design and highlighted in the existing literature [4-7]. This is because the service temperatures of CFRP-strengthened steel structures may vary significantly due to seasonal and diurnal temperature changes. Sometimes, when the surface of the CFRP plate is directly exposed to solar radiation (such as in the strengthened steel structures used in outdoor applications), it is possible to obtain relatively high service temperatures (i.e., around 60°C) at the bond interface, which are much higher than the room temperature of the air [5,7,8]. In addition, the EB CFRP-strengthened steel structures may suffer from severe cold environments in winter, especially when used in high latitudes [9,10].

The adhesives widely used to bond CFRP plates to steel structures are usually epoxy resins, mainly because of their excellent mechanical properties and workability. Apart from the preceding advantages, however, the material properties of conventional epoxy adhesives are sensitive to service temperature variations. At relatively high service temperatures, epoxy adhesives may change from a solid-state to a softened and viscous state. For commercially available epoxy resins used in the strengthening applications, the reported glass transition temperature is typically 40-60°C [11,12]. When the epoxy adhesives are subjected to service temperatures close to the glass transition temperature, their strength and stiffness may be significantly reduced. Also, epoxy adhesives may become brittle at low service temperatures, possibly leading to stress concentrations at the bond interface due to the increased stiffness and reduced deformability of epoxy adhesives. Therefore, the debonding load (also referred to as "bond strength" or "ultimate load" in the literature) of the EB CFRP plate and the steel substrate can be severely affected by the service temperature variations. In addition to the mechanical property changes of epoxy resins, interfacial thermal stresses may be generated during service

temperature variations due to the different coefficients of thermal expansion (CTEs) of steel and CFRP materials. The existing studies have only investigated the thermal stress effects through analytical solutions and finite element (FE) modeling [13-22]. The results have indicated that the interfacial thermal stresses were possibly in the same or opposite directions as that generated by the mechanical loading, resulting in a decrease or increase in the debonding load of the bond interface.

## 2. Existing Experimental and Analytical Studies

A few CFRP-to-steel bonded joints [11,23-30] were tested under combined pull-out loads and high temperature variations (i.e., thermal loadings) in the literature, aiming to study the temperature-dependent bond properties of the CFRP-to-steel interface. For example, Zhou *et al.* [29] carried out pull-out tests on CFRP-to-steel single-lap bonded joints at the service temperatures from 25°C to 55°C. The test results showed that the initial stiffness and peak shear stress of the bond interface decreased at high service temperatures. However, the interfacial fracture energy increased with temperatures up to 47.5°C and then reduced with the further temperature increase. Biscaia *et al.* [30] reported an average 65.9% reduction in the debonding load for the bonded joints tested at high temperatures of 80°C and 95°C compared to the results obtained at 20°C. Meanwhile, a 90.1% decrease in the peak shear stress and a 61.0% decrease in the ultimate slip were observed. Similar phenomena were also reported in other pull-out tests [11,23-28].

Heshmati *et al.* [12] conducted a literature review work and collected the results from some previous bonded joint tests [24,25,31], which showed that the initial (elastic) stiffnesses of the bond interface decreased from room temperature to $T_g$-5°C ($T_g$ was the glass transition temperature of the bonding adhesive), while the debonding loads maintained almost unchanged within the temperature range. However, when the exposure temperatures were higher than $T_g$-5°C, the debonding loads and elastic stiffnesses of the bond interface gradually decreased with average rates of 3.3% and 4.4% per degree Celsius, respectively. In contrast, the pull-out tests of CFRP-to-steel bonded joints at decreased temperatures (i.e., low service temperatures changed from curing temperature under ambient conditions) are limited [32]. The results of the pull-out tests showed that the elastic stiffness and peak shear stress of the bond interface remained nearly constant or increased slightly at decreased temperatures. Similar observations were also reported for the bond interface between EB FRP composites and concrete or other substrates when epoxy resins were used as the bonding adhesives [33-36]. Moreover, the

debonding load of the joint was related to the interfacial fracture energy (defined as the area enclosed by the shear stress versus the interfacial slip relationship) if the bond length was sufficiently long and larger than the effective bond length (i.e., the length beyond which the debonding load of the joint would not increase any further). However, it was observed that the deformability of epoxy resins decreased significantly at low service temperatures, resulting in brittle bond failures [32,33,35] and reduced interfacial fracture energy [33]. In addition to the pull-out tests, some analytical solutions were proposed to predict the full-range deformation behavior of FRP-to-concrete bonded joints under combined thermal and mechanical loadings [13-15,22]. These analytical approaches are also applicable to CFRP-to-steel bonded joints and can be used to isolate the effect of interfacial thermal stresses from the changes in bond properties, since only the latter should be appropriately considered when developing temperature-dependent bond-slip models of the bond interfaces [20,22].

From the literature review work described above, the majority of the bonded joint tests are carried out at increased temperatures (i.e., representing ambient conditions where the service temperatures are much higher than the curing temperature), while there is lacking bonded joint tests of the CFRP-to-steel interface at decreased temperatures (i.e., lower winter service temperatures). More importantly, reliable bond-slip models for CFRP-to-steel interfaces at different service temperatures are lacking in the literature, mainly because the local bond-slip relationships of the bond interfaces tested in previous studies have not been reported in detail. This paper presents a comprehensive experimental study on the pull-out tests of CFRP-to-steel bonded joints at increased and decreased service temperatures. The experimental results of debonding loads and strain distributions of the CFRP plate at different service temperatures are investigated and compared. The latter is used to derive the local bond-slip model of the CFRP-to-steel interface at different service temperatures. Then, a finite element (FE) model is developed to predict the bond behavior of the CFRP-to-steel interface under mechanical loading and temperature variations, in which the preceding bond-slip model is used to define the local shear stress versus the interfacial slip relationships of the interface at different service temperatures. The proposed FE model is validated by the pull-out tests in the paper and then used to further study the temperature effects on the interfacial shear stress distributions and the debonding loads of the bonded joints at different service temperatures.

## 3. Experimental Program

### *3.1. Material properties*

A series of CFRP-to-steel double-lap bonded joint tests were carried out at five different service temperatures of -20°C, 0°C, 30°C, 45°C and 60°C, and accordingly, the specimens were named as JT-20, JT0, JT30, JT45 and JT60, respectively. At each service temperature, three duplicated specimens were prepared and identified by a letter of "A", "B" or "C" after the specimen designation. These five different temperatures were determined to reflect possible service temperature variations that CFRP-strengthened steel structures may encounter in different regions of China [19]. **Fig. 1** shows the geometric dimensions of the double-lap bonded joint, which consists of two separate steel plates jointly bonded with CFRP plates on both surfaces. The length of the two CFRP plates was 340 mm, and the bond lengths were 150 mm on each steel plate, leaving a gap of 40 mm between the two ends of the steel plates (see **Fig. 1** for more details).

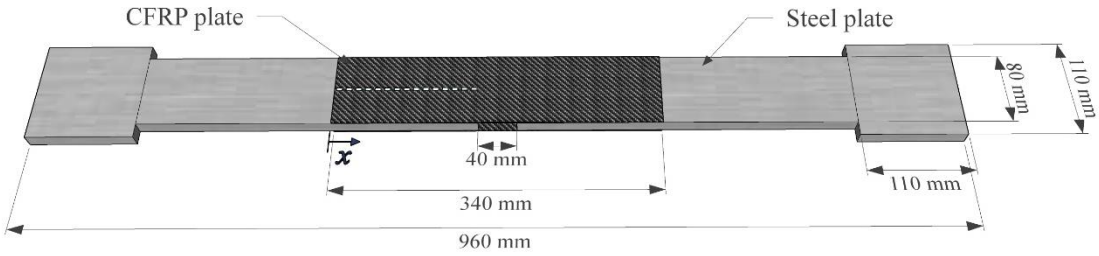


**Fig. 1**. Geometric dimensions of the double-lap bonded joint

The steel plates were made of Q235 steel with a thickness of 15 mm, and the width of the bonding area was 80 mm. The two ends of the steel plate were wider (i.e., 110 mm) and used to apply the pull-out force from the grip by friction. The nominal thickness of the CFRP plate was 1.5 mm. The elastic modulus and ultimate strain were measured as 141.9 GPa and 13050 με as per ASTM D3039 [37]. In addition, the elastic modulus, yielding stress and tensile strength of the steel were determined to be 204.6 GPa, 225.9 MPa and 370.5 MPa as per ASTM A370 [38]. The thermal expansion coefficients of CFRP plate and steel were measured as $4.2\times10^{-6}$/°C and $10.4\times10^{-6}$/°C according to the test standard of ISO 11359-2 [39].

The bonding adhesive used in the pull-out tests was Sikadur-330CN adhesive. According to the brochure provided by the manufacturer, the tensile strength and elastic modulus of the adhesive at room temperature were 49.7 MPa and 2.55 GPa, respectively. The $T_g$ value of the adhesive was measured by dynamic mechanical analysis (DMA) as per ASTM D7028 [40]. **Fig. 2** depicts the changes of storage (elastic) modulus, modulus loss and tan($\delta$) (defined as the ratio of modulus loss divided by storage modulus) with temperatures. It is noteworthy that there

are three different methods usually used to define the $T_g$ value, including the $T_g$-onset method, the peak in the loss modulus curve and the peak in the tan($\delta$) curve. A full description of these definitions is beyond the scope of the current study and more details can be found in Gao *et al.* [41] and Maluk *et al.* [42]. As shown in **Fig. 2**, the $T_g$ values using the $T_g$-onset method, the peak in the loss modulus curve and the peak in the tan($\delta$) curve are determined as 56.25°C, 60.15°C and 69.74°C, respectively.

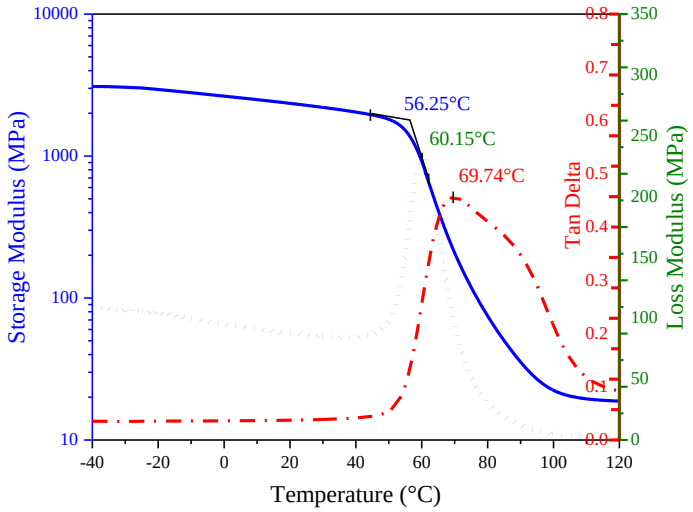


**Fig. 2**. Different methods used for determining the $T_g$ values

### *3.2. Strengthening applications*

Both surfaces of each steel plate were firstly smoothened using a steel grinder. Then, the steel surfaces were degreased with acetone and sandblasted to remove the oxide coating (**Fig. 3a**). According to the suggestion specified in Fernando *et al.* [43], angular alumina grits with a diameter of 0.25 mm were used for sandblasting to ensure the chemical compatibility of the steel surfaces with the bonding adhesive. In addition, the blasting angle was controlled at about 75° [44], and the pressure was maintained at around 0.4-0.6 MPa. After sandblasting, the residual surface dust was cleaned by using compressed air. Before bonding to the steel surfaces, the CFRP plates were carefully washed with acetone using gauze. Then, the CFRP plates were bonded to the steel surfaces within half an hour to avoid oxidation of the steel surfaces. As Deng and Lee [45] recommended, more adhesives were laid along the center than the outer edges, which allowed air trapped between the adherends to be easily escaped when they were pushed together. The excess adhesives along the edges of the plate were scraped off, collected and weighted. The average epoxy weight per side of the bonded joint was 11.4 g, and the average thickness was determined as 0.37 mm by dividing the weight by the epoxy density. The bonded joints were cured at room temperature for at least two weeks after the strengthening

application was completed. During the curing process, the uniform thickness of the adhesive layer was maintained by applying consistent compressive stress of approximately 4.2 kPa on the top surface of the CFRP plate (by applying a weight as shown in **Fig. 3b**). Such a curing method was also used by Zeng *et al.* [46] and Colombi *et al.* [47] for the preparation of the CFRP-strengthened steel beams.

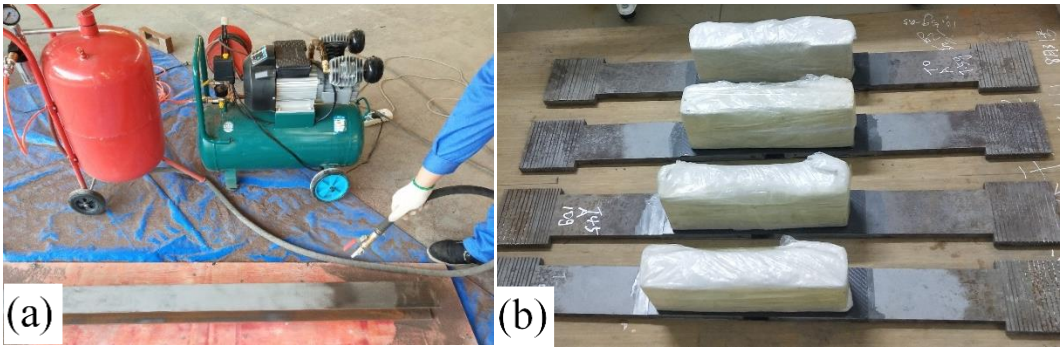


**Fig. 3**. Preparation of the specimens: (a) sandblasting; (b) curing.

### *3.3. Loading scheme and instrumentation*

**Fig. 4** shows the test setup and environmental chamber used for the pull-out tests. The environmental chamber was equipped with several internal insulation panels to reduce possible heat exchange between it and the surrounding air. During the tests, high service temperatures were achieved by the heating pipes, while low service temperatures were obtained using liquid nitrogen. Three thermocouples were mounted at various locations on each bonded joint, including two end zones of each specimen and the mid-height of the CFRP plate, to ensure that the bonded joint reached a uniform temperature equal to the target service temperature.

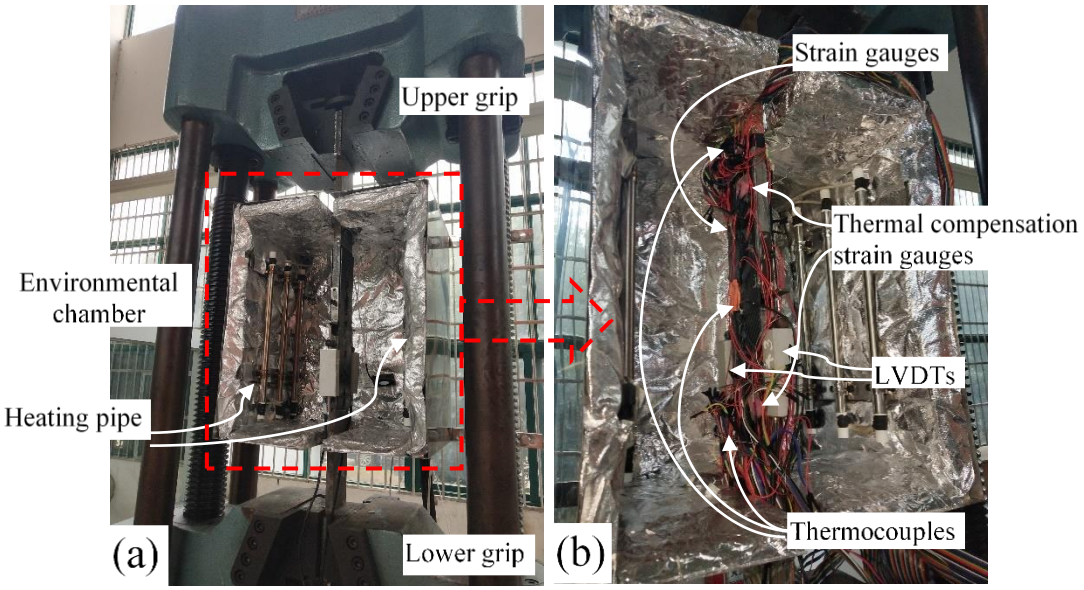


**Fig. 4**. Test setup and environmental chamber: a) overview; b) inside view.

At each service temperature, several strain gauges were bonded to the surfaces of the CFRP plate in the first specimen of three duplicates to measure the strain distributions in the CFRP plate. The arrangement and detailed locations of the strain gauges are shown in **Fig. 5**. The first strain gauge was located 5 mm from the plate end, and the others were spaced at 10 mm intervals apart (**Fig. 5**). The other two strain gauges from the same batch were bonded to TiS glasses and placed near the joint to account for thermal compensation. As shown in **Fig. 5**, two LVDTs were attached to the adjacent ends of two steel plates with a gap of 40 mm to measure the relative displacement. Therefore, the measured displacements consisted of two parts, including the sum of the interfacial shear slips at the two loaded ends and the axial deformation of the 40 mm unbonded length of the CFRP plate. Therefore, half of the measured relative displacement minus the axial deformation of the 20 mm CFRP plate was the slip at the loaded end of the bonded joint under combined thermal and mechanical loadings.

The testing procedure was divided into two steps. First, the bonded joint was placed in the environmental chamber with the upper end held by the loading grip. Then the heating pipe or liquid nitrogen pump was started to increase or decrease the chamber temperature to the target service temperature. The pull-out loading was applied within 30 min after the measured temperatures were stabilized at the target temperature and evenly distributed across the different positions recorded by the thermocouples. The pull-out load was applied by the lower grip at a speed of 2 mm/min.

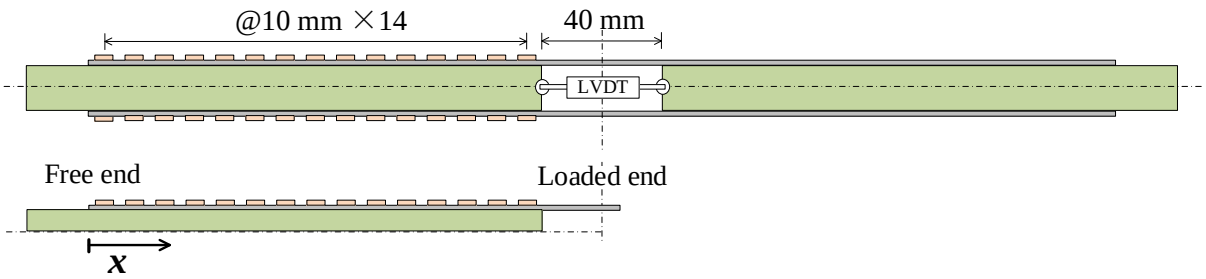


**Fig. 5**. Locations of strain gauges and LVDTs

## 4. Results and Discussion

### *4.1. Failure modes*

**Fig. 6** shows a typical failure mode of the bonded joints tested at different service temperatures from -20°C to 45°C, which was caused by the debonding failure at the bond interface and the localized delamination of the CFRP plate. This failure mode has demonstrated an excellent surface preparation of the steel substrate. However, when the service temperature was increased to 60°C, the delamination zone of the CFRP plate became negligible, mainly due

to the softening of the bonding adhesive at the high service temperature close to the glass transition temperature of the adhesive. Similar observations were also reported in the previous pull-out tests of CFRP-to-steel bonded joints at high service temperatures [24,26]. **Fig. 7** further compares the difference between the failure modes of JT0-A and JT60-A after the pull-out tests. It can be seen that a large number of burrs and adhesive fragments were attached to the debonded interface of JT0-A, and the observed failure progress was very brittle. In contrast, the debonded surface of JT60-A was relatively smooth because of the reduced elastic stiffness and softening behavior of the adhesive layer at 60$^{o}$C.

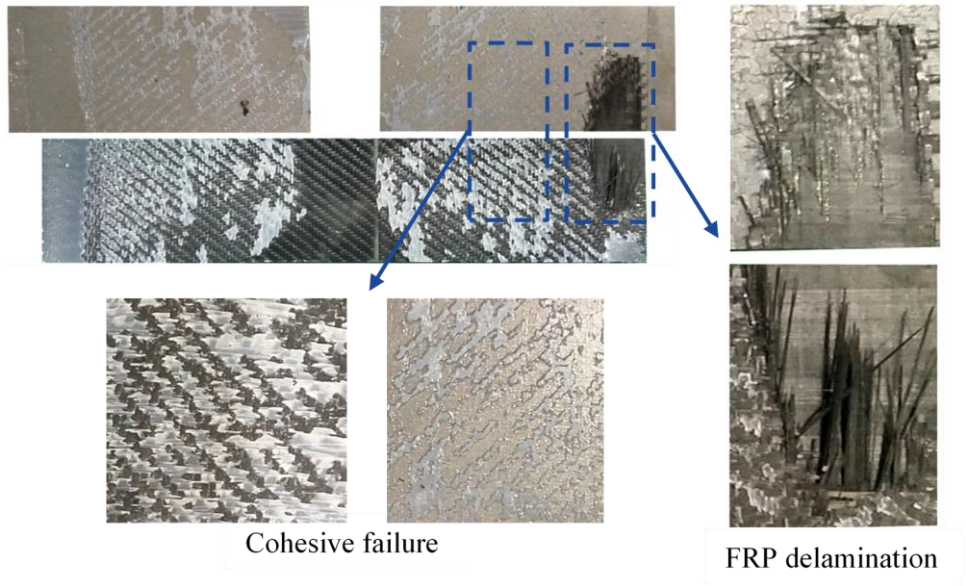


**Fig. 6**. Debonded interface of JT-20-A.

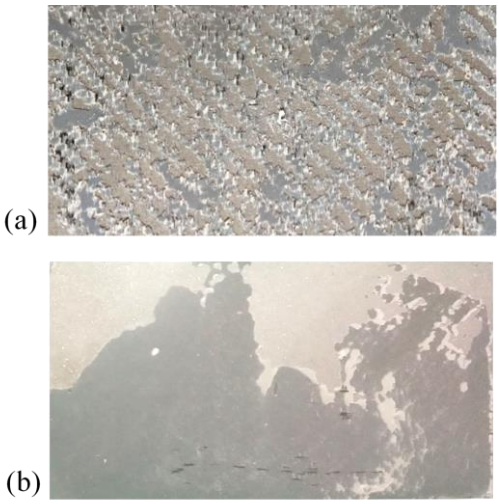


**Fig. 7**. Difference between the failure modes of: (a) JT0-A; and (b) JT60-A.

### *4.2. Experimental results*

**Fig. 8** shows the changes of debonding loads for the CFRP-to-steel bonded joints tested at different service temperatures. In this figure, the existing pull-out test results of CFRP-to-steel bonded joints reported in the literature [24-30,32] are also presented for comparison. It can be seen that most of the existing pull-out tests were conducted at high service temperatures, as mentioned earlier. All the debonding loads are normalized by the corresponding average value measured at room temperature for a clear comparison. In **Fig. 8**, since different types of bonding adhesives were used in the pull-out tests of He *et al.* [26] and Al-Shawaf *et al.* [25,32], the debonding loads at different service temperatures are normalized by the average value of the joints obtained at room temperature for each type of adhesive, and the results of different types of adhesives are denoted by various symbols. In addition, only the specimens cured at room temperature in Chandrathilaka *et al.* [28] are included in the figure for comparison.

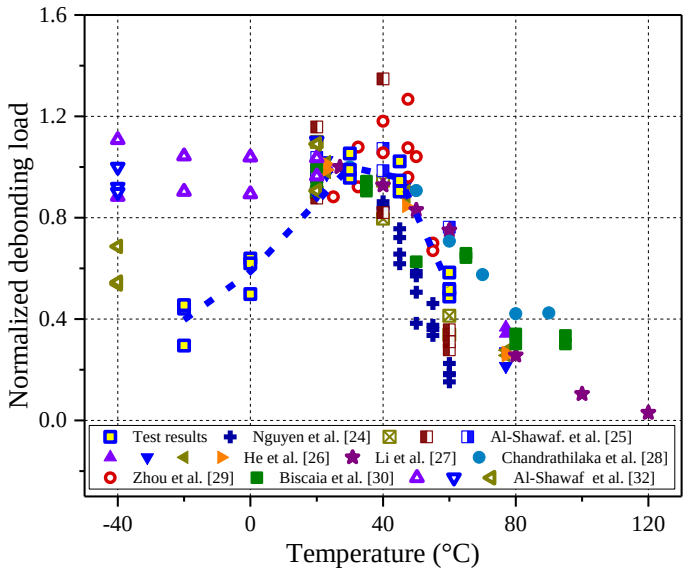


**Fig. 8**. Comparison of the normalized debonding loads at different service temperatures

In the present study, the debonding loads increased from -20°C to 30°C and then decreased with the further service temperature increase. The average debonding loads were reduced only slightly (i.e., 4.3%) from 30°C to 45°C and more significantly (i.e., 44.7%) from 45°C to 60°C. The latter significant reduction of the debonding loads is attributed to the softening behavior of the adhesive layer at high service temperatures close to its glass transition temperature. Similar observations about the significant reduction of the debonding loads for the bonded joints tested at high service temperatures were also reported by other researchers [24-30], in which epoxy resins were used as the bonding adhesives. In addition, the debonding loads of the joints decreased significantly from the room temperature (i.e., 30°C in this study)

to low service temperatures (i.e., 0°C and -20°C), although the elastic stiffness of the bonding adhesive was observed to be slightly increased (**Fig. 2**). Therefore, the debonding load reduction was due to the combined effects of reduced interfacial fracture energy and interfacial thermal stresses. Such combined effects will be further examined and discussed in the following sections to clarify how they affect the bond behaviors of CFRP-to-steel bonded joints under combined mechanical and thermal loadings (i.e., service temperature variations).

Furthermore, current design guidelines recommend that the maximum service temperature (i.e., temperature limit) specified for FRP-strengthened structures should be less than $T_g$-15°C [48,49]. According to the above design guidance, the allowable maximum service temperature of the adhesive used in the present study should be 41°C, 45°C or 55°C according to the $T_g$ value determined by the $T_g$-onset method, the peak value of the loss modulus curve or the peak value of the tan($\delta$) curve, as described in **Section 3.1**. The test results in **Fig. 8** have indicated that the recommended maximum service temperature for practical FRP strengthening applications is generally safe when the $T_g$ value is determined using the $T_g$-onset method or the peak in the loss modulus curve method. However, since the debonding loads were significantly reduced at 55°C, this design guidance may not be conservative for practical FRP strengthening applications when the $T_g$ value is determined as the peak in the tan($\delta$) curve (i.e., 55°C in the current study). This observation suggests that more attention should be paid to the method used for determining the $T_g$ value for practical strengthening applications. In addition, the significant reduction of the debonding loads at low service temperatures raise safety concerns for the applications of FRP-strengthened steel structures in cold regions.

**Fig. 9** compares the load-displacement curves of the bonded joints tested at different service temperatures. Since the measured curves for the three duplicates tested at each temperature are similar (see **Fig. 17** for more details), only the results of the first specimen are included herein for a clear comparison. At low service temperatures of 0°C and -20°C, the load-displacement curve exhibits an almost linear elastic response until the debonding failure of the CFRP plate. At service temperatures of 30°C and 45°C, the pull-out load initially grows linearly with the displacement in the elastic stage. With a further increase in the displacement, a nonlinear load-displacement response appears and reaches a short load plateau, and the load increase converges at the debonding failure. This load plateau indicates that the bond length used in the study was longer than the "effective bond length" of the bonded joint. However, this load plateau was not observed at 60°C, because such temperature led to the increase in the effective bond length (i.e., longer than 150 mm used in this study). The increase in the effective

bond length at high service temperatures is mainly attributed to the decrease in elastic stiffness and the associated softening behavior of the bonding adhesive [7,29]. Another reason for the increase in the effective bond length at high service temperatures is the effect of interfacial thermal stresses caused by the different CTEs of CFRP and steel plate, which requires a longer bond length to reach the load capacity (i.e., debonding load) as revealed by the analytical solution proposed by the authors [14]. In addition, the initial slopes of the load-displacement curves were slightly larger at low service temperatures due to the increased elastic stiffness of the bond interface (see **Table 1** for more details).

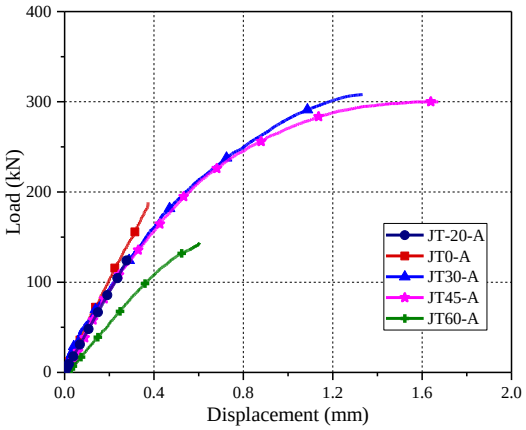


**Fig. 9**. Load-displacement curves of the bonded joints tested at different service temperatures

**Fig. 10** shows the strain distributions in the CFRP plate of the bonded joint tested at 30°C, in which the *x*-axis originates from the free end (**Fig. 5**). It is evident that the strain values at each location grow with the applied pull-out loads. Furthermore, the CFRP strains increase monotonically from the free end ($x$=0 mm) to the loaded end ($x$=150 mm). At the ultimate state, the strain distribution curve is almost flat near the loaded end, indicating that the interfacial debonding of the CFRP plate occurred in the loaded end region. **Fig. 11** further compares the strain distributions in the CFRP plate for the joints tested at different service temperatures under the same pull-out load (i.e., 100 kN). The recorded CFRP strains near the loaded end (at $x$ =145 mm) are very close, while the variation trends of the strain distributions along the bond length are dissimilar at different service temperatures. At low service temperatures, the strain distributions grow slowly from the free end and increase abruptly near the loaded end, whereas at 60°C the CFRP strains are increased almost linearly from the free end to the loaded end. The different strain distributions should be due to diverse local bond-slip relationships of the bond interface at different service temperatures, which will be further examined in the next section.

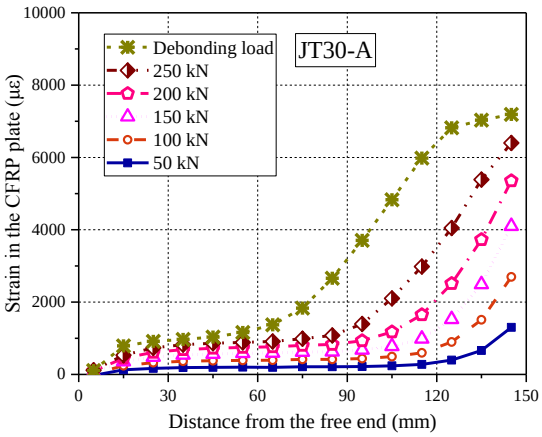


**Fig.10**. Strain distributions in the CFRP plate of JT30-A.

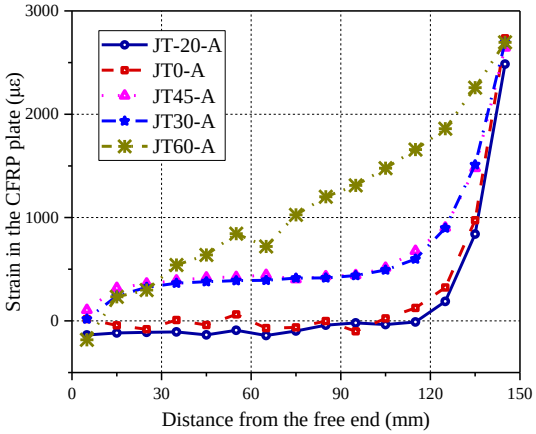


**Fig. 11**. Strain distributions in the CFRP plate at 100 kN.

### *4.3. Local bond-slip relationships*

The interfacial bond stress ($\tau_{i+\frac{1}{2}}$) ($i$ starts from the free end) between two adjacent strain gauges at the locations of $x_i$ and $x_{i+1}$ can be derived from the difference of the measured strains (i.e., $\varepsilon_{i+1} - \varepsilon_i$) by the following equation [1,50-52].

$$\tau_{i+\frac{1}{2}} = \frac{\varepsilon_{i+1}-\varepsilon_i}{x_{i+1}-x_i} E_f t_f \quad (1)$$

where $E_f$ and $t_f$ are the elastic modulus and thickness of the CFRP plate. The corresponding local interfacial slip can be calculated by integrating the CFRP strain from the free end to the relevant location as follows:

$$\delta_{i+\frac{1}{2}} = \sum_1^i \frac{\varepsilon_i+\varepsilon_{i+1}}{2} (x_{i+1} - x_i) \quad (2)$$

**Fig. 12** shows the local bond-slip relationships obtained from the pull-out tests at different service temperatures. The dotted lines represent the results recorded at various locations along the CFRP plate, while the dashed lines are based on nonlinear regression analysis using the curve fitting toolbox provided by MATLAB software. The same data treatment approach was also used by the previous study to derive the local bond-slip relationships of the CFRP-to-steel interface [29].

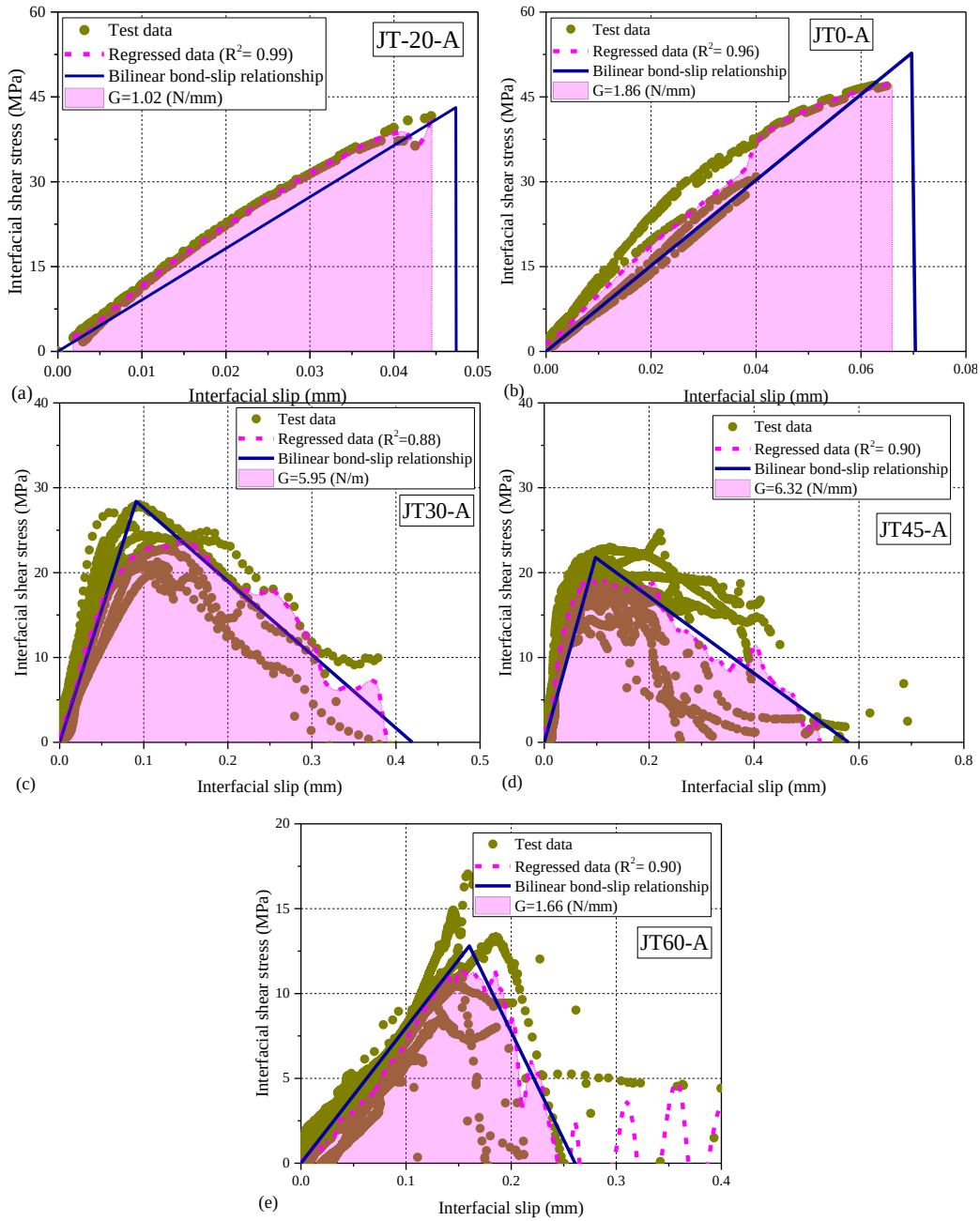


**Fig. 12**. Local bond-slip relationships obtained from the bonded joint tests: (a) JT-20-A; (b) JT0-A; (c) JT30-A; (d) JT45-A; (e) JT60-A.

From the measured and regressed curves shown in **Fig. 12**, a bilinear relationship can be used approximately to describe the local bond-slip responses at different service temperatures. Indeed, due to the increased elastic stiffness of the bonding adhesive at low service temperatures, the local bond-slip relationships of the joints tested at -20°C and 0°C exhibit a very brittle behavior with an abruptly descending portion. That is, the bilinear bond-slip model can be simplified to an elastic-brittle model, as illustrated in **Fig. 12a** and **12b**. **Fig. 13** depicts the bilinear bond-slip model used to describe the relationship between the shear stress and the interfacial slip, including elastic and softening portions (**Fig. 13a**). In the elastic stage (i.e.,

$\delta<\delta_0$ and $\tau<\tau_p$), the shear stress increases linearly with the interfacial slip with a constant slope of $K_T$. After reaching the peak shear stress ($\tau_p$), the interfacial shear stress decreases linearly with the interfacial slip with a slope of $K_T'$ until the interfacial debonding occurs at the slip $\delta_f$.The interfacial fracture energy is defined as the area underneath the bond-slip curve (i.e., $G_f = \tau_p \delta_f/2$). As mentioned earlier, at -20°C and 0°C, the interfacial shear stress is observed to increase linearly to $\tau_p$, followed by the CFRP debonding failure (i.e., $\delta_0=\delta_f$), and thus the bond-slip model can be approximately described by the elastic-brittle model as shown in **Fig. 13b**.

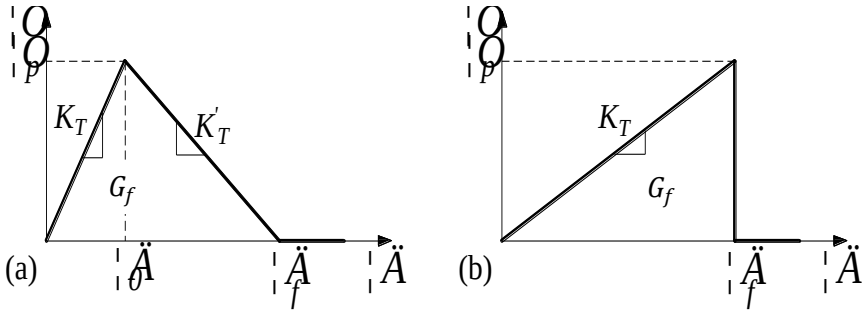


**Fig. 13**. Local bond-slip relationships: a) bilinear; b) elastic-brittle.

The area enclosed by the regressed shear stress-interfacial slip curve in **Fig. 12** is used to define the interfacial fracture energy for the local bond-slip model, while the slopes of the elastic and softening portions ($K_T$ and $K_T'$) are determined from the least-squares curve fitting of the regressed curve at each service temperature. For the joints tested at -20°C and 0°C, only the elastic stiffness ($K_T$) needs to be determined. **Table 1** summarizes all the bond properties of the CFRP-to-steel interface at different service temperatures obtained from the test results presented in **Fig. 12**. It can be seen that the elastic stiffness and peak shear stress are generally reduced with the service temperature increase, while the interfacial fracture energies at 30°C and 45°C are much higher than those obtained at other service temperatures.

**Table 1**. Bond properties of the interface at different service temperatures

| Temperature (°C) | Elastic stiffness (MPa/mm) | Peak shear stress (MPa) | Interfacial fracture energy (N/mm) |
|---|---|---|---|
| -20 | 910.3 | 42.92 | 1.02 |
| 0 | 757.1 | 52.74 | 1.86 |
| 30 | 312.4 | 28.39 | 5.95 |
| 45 | 223.1 | 21.79 | 6.32 |
| 60 | 79.9 | 12.77 | 1.66 |

## 5. Finite Element (FE) Model

### *5.1. Description of the FE model*

To gain insight into the temperature effects on the bond behavior of CFRP-to-steel bonded joints at different service temperatures, a two-dimensional finite element (FE) model was developed within the framework of ABAQUS 6.14. The CFRP and steel plates were modeled by 4-node plane stress quadrilateral elements (CPS4R), while the adhesive layer was modeled by a 4-node cohesive element (COH2D4). The element sizes of the CFRP and steel plates as well as the adhesive layer were set as 0.2 mm [16]. Due to the symmetry of the bonded joint, only a quarter of the joint was modeled (**Fig. 14**). The symmetrical boundary conditions in the vertical and horizontal directions were set on the right and bottom of the FE model, respectively. The room temperature was set to 30°C as the initial step. The service temperature was defined as a second loading step using the predefined field variable, in which the entire joint was set as the same service temperature without considering the temperature gradient within the joint. This assumption was established corresponding to the final state after completing the service temperature change. Then, pull-out loads were applied using a displacement-controlled manner at the end of the steel plate. In the FE model, the CFRP and steel plates were assumed to be isotropically elastic with the stiffnesses of 141.9 GPa and 204.6 GPa, respectively. The local bond-slip relationships of the CFRP-to-steel interface at different service temperatures were defined by the bond properties provided in **Table 1**. It is worth noting that for the FE modeling process of the joints tested at -20°C and 0°C, the stiffness of the softening portion (i.e., $K_T'$) was defined by a sufficiently large value (i.e., 100 times of $K_T$) to avoid possible numerical convergence problems.

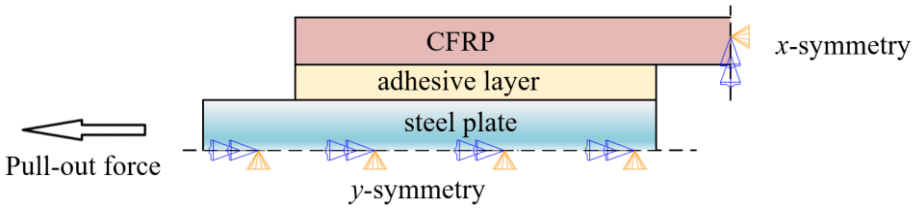


**Fig. 14**. FE model of the CFRP-to-steel bonded joint

### *5.2. Validation of the FE Model*

#### *5.2.1. Distribution of CFRP strains*

**Fig. 15** compares the CFRP strain distributions obtained from the pull-out tests and the FE predictions for the joints under different load levels and service temperatures. The excellent agreement between them has demonstrated the accuracy and reliability of the proposed local bond-slip model that can be used to describe the bond properties of the CFRP-to-steel interface

at different service temperatures. At low service temperatures (e.g., -20°C and 0°C), the CFRP strains grow slowly from the free end and increase abruptly near the loaded end, mainly due to the high shear stiffness and elastic-brittle behavior of the bond interface at low service temperatures. At high service temperatures (e.g., 45°C and 60°C), the CFRP strains increase faster from the free end to the loaded end, and eventually a strain plateau is observed near the loaded end corresponding to the debonding failure of the CFRP plate. The strain distributions have indicated the nonlinear local bond-slip behavior of the bond interface at high service temperatures.

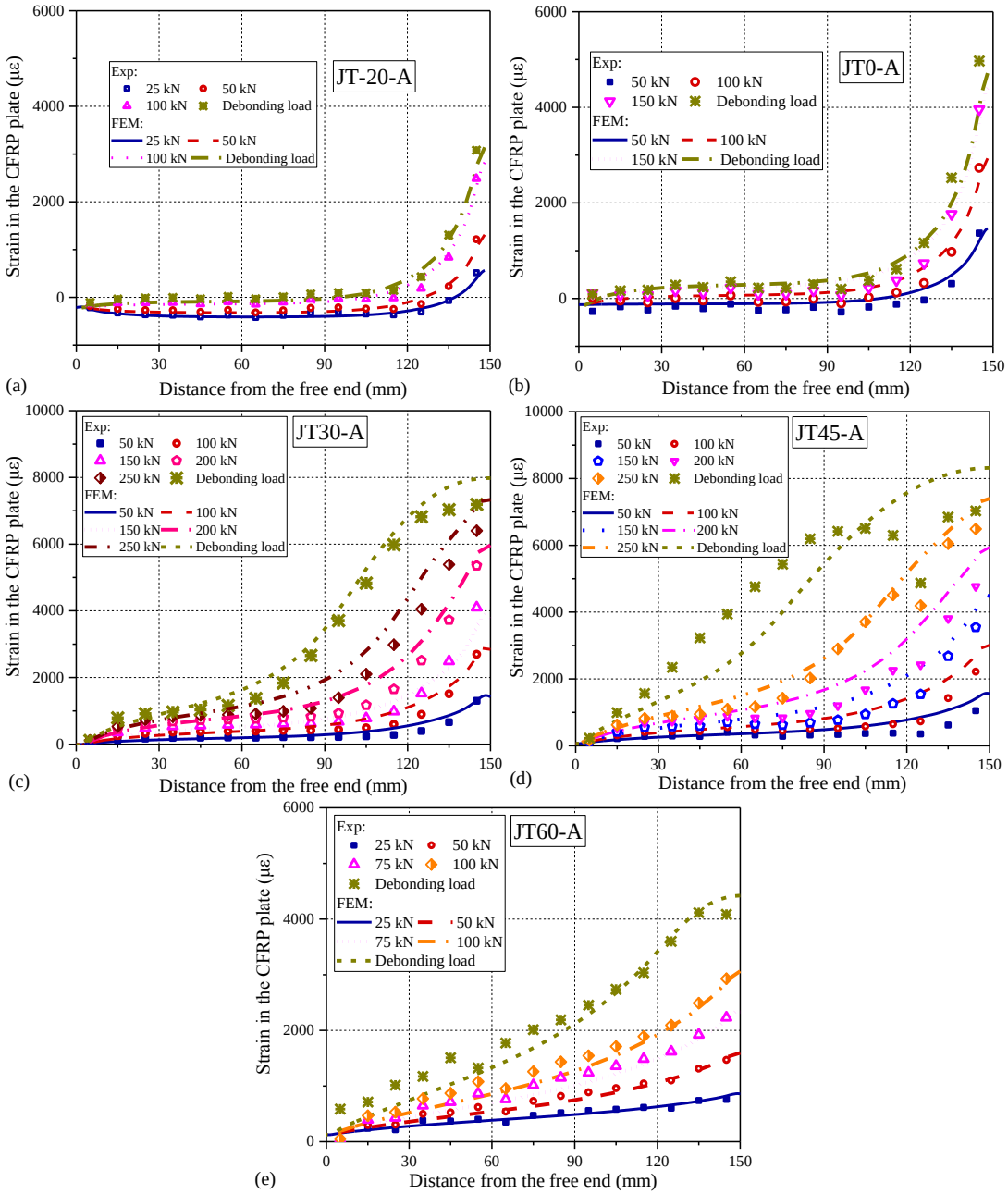


**Fig. 15**. Comparisons of CFRP strain distributions at different load levels obtained from the pull-out tests and the FE predictions: a) JT-20-A; b) JT0-A; c) JT30-A; d) JT45-A; e) JT60-A.

### *5.2.2. Distribution of interfacial shear stresses*

**Fig. 16** further compares the distributions of the interfacial shear stresses obtained from the pull-out tests and the FE model predictions. With the growth of the pull-out load, the bond interface undergoes two stages before the debonding failure, including elastic and elastic-softening stages. At low load levels, the interfacial shear stresses are increased monotonically from the free end to the loaded end, and the entire bond length is in the elastic stage. With the further increase of the pull-out load, the shear stress at the loaded end reaches the peak value and then decreases accordingly, and thus the bond interface enters the elastic-softening stage. Under the ultimate state, the debonding failure occurs at the loaded end of the CFRP plate. Overall, the FE predictions agree well with the test results, although the dispersion between them becomes relatively significant after the bond interface enters the softening stage. It is worth noting that before the pull-out load is applied (i.e., 0 kN), the interfacial shear stresses are distributed almost symmetrically due to the imposition of the service temperature (**Fig. 16a, 16b, 16d and 16e**). The thermal stresses generated near the loaded end at low service temperatures are positive and vice versa, resulting in significant effects on the bond behavior and the associated debonding loads of the joint at different service temperatures, which will be further discussed in the next section.

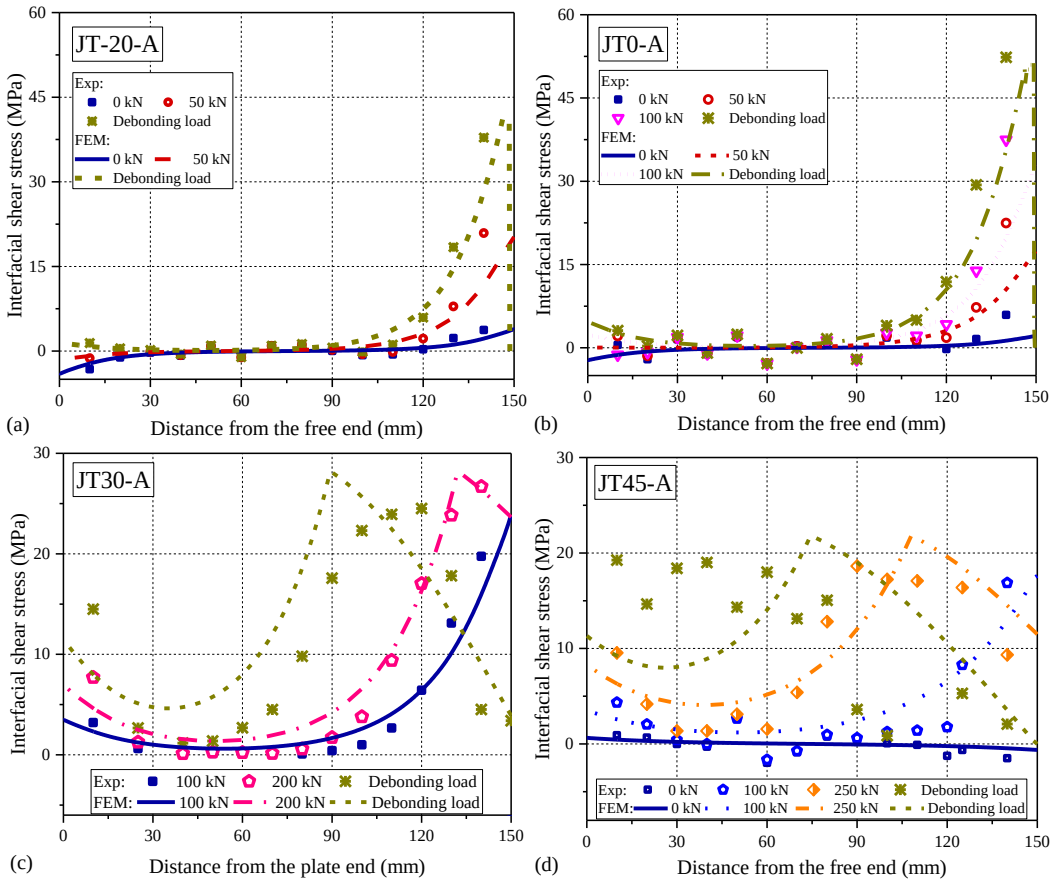

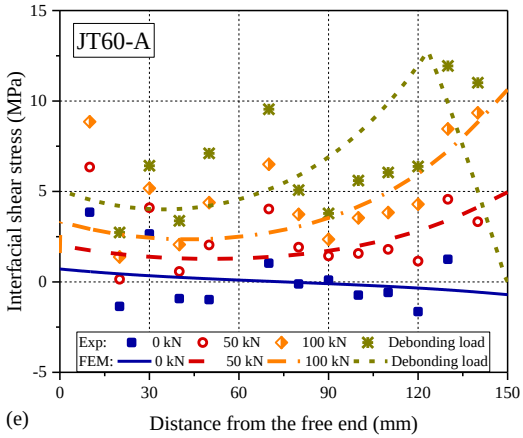


**Fig. 16.** Comparisons of interfacial shear stress distributions at different load levels obtained from the pull-out tests and the FE predictions: a) JT-20-A; b) JT0-A; c) JT30-A; d) JT45-A; e) JT60-A.

### *5.2.3. Load-displacement curves*

**Fig. 17** depicts the comparisons of the load-displacement curves between the pull-out test results and the corresponding FE predictions. All the test results for three duplicate specimens tested at each service temperature are presented, and the debonding loads predicted by the FE model are marked in the figure. It can be observed that in the elastic stage, the load increases linearly with the displacement. At room and high service temperatures, the interfacial deformation process evolves from an elastic stage to an elastic-softening stage, and finally CFRP debonding occurs at the end of the elastic-softening stage. In contrast, at -20°C and 0°C, the elastic stage is approximately terminated at the occurrence of the CFRP debonding, indicating that the elastic-softening stage is negligible due to the increased elastic stiffness of the bond interface at low temperatures. The FE model can accurately predict the load-displacement responses at different service temperatures. Each predicted load-displacement curve is almost the average of the measured results of the three duplicates at each service temperature.

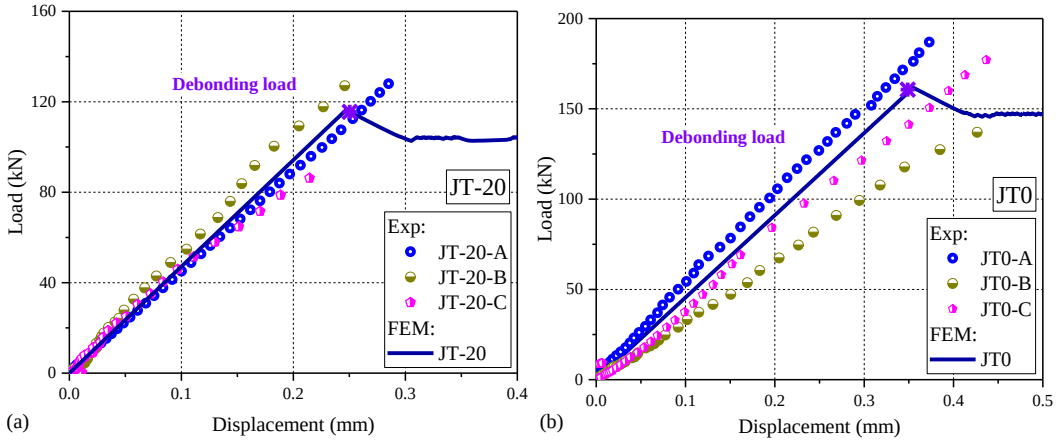

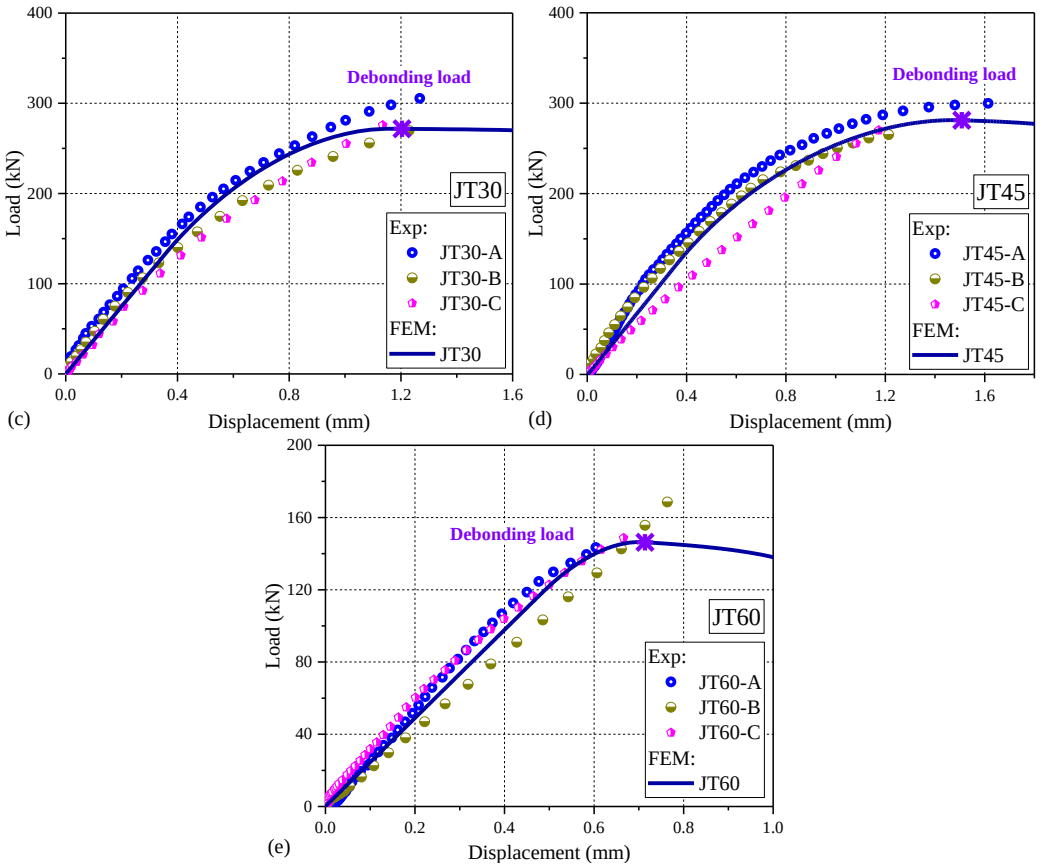


**Fig. 17.** Comparison of load-displacement curves obtained from the pull-out tests and the FE predictions: a) JT-20; b) JT0; c) JT30; d) JT45; e) JT60.

**Table 2** summarizes the debonding loads obtained from the pull-out tests and the FE predictions for the joints tested at different service temperatures. The tested debonding load at each temperature is averaged from the results of three duplicate specimens. The percentage difference between the test result and the corresponding FE prediction is determined by dividing the difference by the tested debonding load. The comparison in **Table 2** shows that the percentage differences are all less than 8%, indicating that the FE model is capable of predicting the debonding loads of the bonded joints tested at different service temperatures.

**Table 2**. Comparison of debonding loads at different service temperatures

| Temperature (°C) | Test results (kN) | FE predictions (kN) | Difference |
|---|---|---|---|
| -20 | 116.5 | 114.8 | 1.9% |
| 0 | 171.9 | 160.7 | 6.1% |
| 30 | 293.5 | 271.7 | 7.5% |
| 45 | 280.9 | 281.2 | -0.1% |
| 60 | 155.5 | 146.3 | 6.0% |

## 6. Discussion of Temperature Effects

### *6.1. Temperature effect on the bond behavior*

**Fig. 18** shows the strain distributions in the CFRP plate after the imposition of the service temperature (i.e., before applying the pull-out load as described in **Section "5.1. Description of the FE model"**), in which the measured CFRP strains and the FE predictions are both included for comparison. Since the applied service temperature at different locations exhibits slight variations along the bond length, the CFRP strain distributions measured by the strain gauges show small fluctuations. Nevertheless, the trends of the measured strain distributions in the CFRP plate at different service temperatures are well captured by the FE model. **Fig. 19** depicts the interfacial shear stress distributions predicted by the FE model. It can be seen that the interfacial shear stresses near the loaded end due to the imposition of the decreased service temperature are in the same direction as the pull-out load. In particular, the maximum value of the thermally induced interfacial shear stresses is about 3.8 MPa when the service temperature is -20°C. This shear stress is approximately 8.9% of the peak shear stress (i.e., 42.9 MPa) obtained during the pull-out test. In addition, the maximum value of the thermally induced shear stresses depends on the range of service temperature variation and the elastic stiffness of the bond interface, as also revealed by the analytical studies proposed by the authors [13,14].

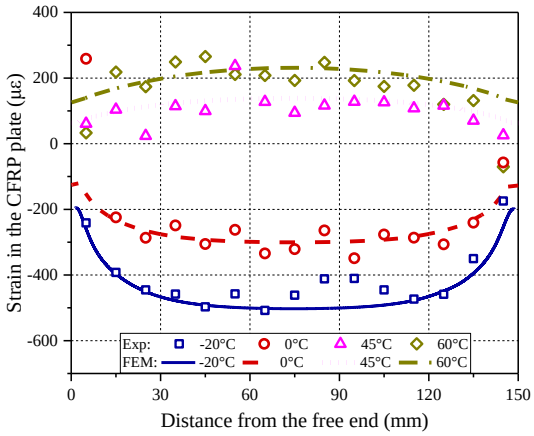


**Fig. 18**. CFRP strain distributions after the imposition of different service temperatures

**Figs. 20 and 21** illustrate the CFRP strain distributions and the corresponding interfacial shear stresses for the bonded joints under a constant pull-out load of 25 kN. Such a load level corresponds to the elastic stage of the bond interface at different service temperatures (as shown in **Fig. 17**). The results obtained at different service temperatures have indicated that they are significantly influenced by the combined effects of mechanical and thermal loadings (i.e., temperature variations). In addition, the comparisons between the measured results and the FE

predictions shown in **Fig. 20** have further demonstrated the reliability of the FE model in predicting the CFRP strain distributions of the joints tested at different service temperatures.

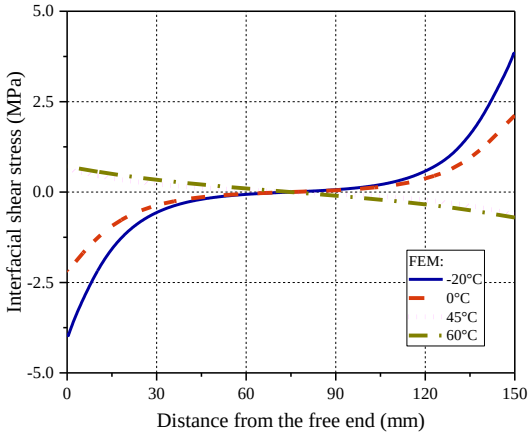


**Fig. 19**. Shear stress distributions after the imposition of different service temperatures

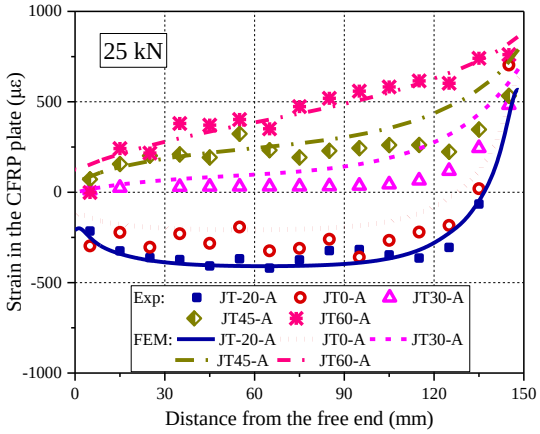


**Fig. 20**. CFRP strain distributions after applying a pull-out load of 25 kN

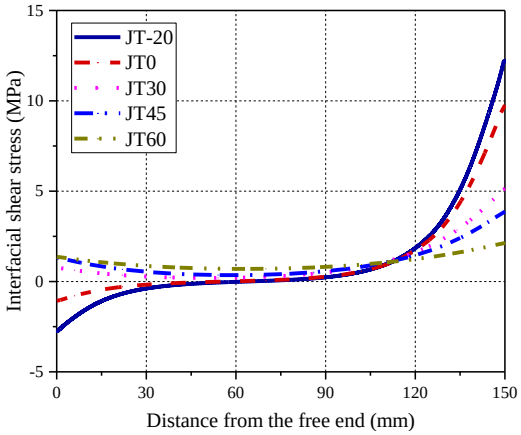


**Fig. 21**. Shear stress distributions after applying a pull-out load of 25 kN

As shown in **Fig. 21**, the interfacial shear stresses at the loaded end are affected by the temperature variations. That is, higher shear stresses are obtained at low service temperatures (i.e., -20°C and 0°C), while the minimum shear stress occurs at 60°C. The latter is attributed to the combined effects of interfacial thermal stress and reduced elastic stiffness of the bond

interface. The observations in **Fig. 21** also suggest that the decreased temperature variations may lead to an earlier occurrence of the debonding failure, and thus more attention should be paid to the CFRP debonding of the strengthened steel beams at low service temperatures.

### *6.2. Temperature effect on the debonding load*

In the analytical solution previously proposed by the authors [13], the effect of interfacial thermal stress on the debonding load of the bonded joint was theoretically analyzed in the case of single-lap shear tests. From the analytical solution, the increase in the debonding load ($\Delta P_{deb}$) due to the presence of interfacial thermal stress can be calculated by the following equation:

$$\Delta P_{deb} = -\frac{E_p t_p b_p}{1+\alpha}(\alpha_p - \alpha_c)\Delta T \quad (3)$$

where $\alpha$ is the stiffness ratio defined as $\alpha = E_p t_p b_p / E_s t_s b_s$. $E, t, b$ are the elastic modulus, thickness and width of the adherend with the subscripts "$p$" or "$s$" representing the CFRP plate or the steel substrate, respectively. According to Eq. (3), the increase in the debonding load induced by the thermal stress depends on the properties of the CFRP plate and the steel substrate; however, it is irrelevant to the local bond-slip behavior of the bond interface.

The present FE model can be used to investigate the temperature effects on the debonding loads of the bonded joints at different service temperatures, in which the combined effects of thermal stresses and local bond-slip behavior (i.e., bond properties) can be properly considered for different temperatures. Therefore, the advantage of the present FE model over the previous analytical solution is that the former can be used to distinguish the above two different effects on the debonding loads. **Fig. 22** compares the change in the debonding load at different service temperatures predicted by the FE model and the analytical solution. Note that the increases in the debonding load are determined by subtracting the load values at different service temperatures from the corresponding analytical or FE result obtained at 30ºC. It can be seen that the analytical results are almost increased linearly with the temperature growths, while the FE results show that the debonding load is reduced significantly at 0°C, -20°C and 60°C. The difference between the analytical results and the FE predictions is mainly due to the changes in the local bond-slip behavior (i.e., bond properties) of the CFRP-to-steel interface at different service temperatures.

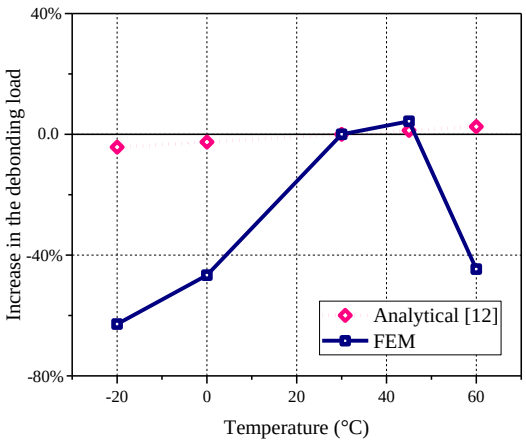


**Fig. 22**. Temperature effects on the debonding loads: Analytical vs. FE results

## 7. Conclusions

This paper presents the results from the pull-out tests of CFRP-to-steel bonded joints at different service temperatures from -20°C to 60°C. The test results including the failure modes, debonding loads, load-displacement curves, CFRP strain distributions and interfacial shear stress and slip responses were examined and compared. Also, a bilinear local bond-slip model was established to describe the shear stress versus the interfacial slip relationships of the bond interface at different service temperatures. An FE model was proposed to predict the bond behavior and the debonding loads of the bonded joint at different service temperatures and was validated through the comparisons between the experimental and FE results. The validated FE model was then used to further investigate the temperature effects on the CFRP strain distributions, interfacial shear stresses and the debonding loads of the bonded joints at different service temperatures. Based on the results and discussions presented in the paper, the following conclusions can be drawn:

(a) The service temperature variations have two different effects on the bond behavior and the related debonding loads of the bonded joint at different service temperatures, including the effect of interfacial thermal stresses and the changes in the local bond-slip behavior.

(b) The debonding loads of the bonded joint are increased from a low service temperature to room temperature and then decrease at a high service temperature close to the glass transition temperature of the bonding adhesive.

(c) The bilinear bond-slip model can be used to describe the relationships between the shear stress and the interfacial slip at different service temperatures. At low service temperatures, the softening portion of the bilinear model can be neglected, and thus the bond-slip model can be simplified as the elastic-brittle model.

(d) The elastic stiffness and the peak shear stress of the local bond-slip model are generally reduced with the service temperature increase, while the interfacial fracture energy decreases at both low and high service temperatures.

(e) The good agreement between the test results and the corresponding FE predictions has demonstrated the reliability and accuracy of the proposed FE model. The advantage of this FE model over the previous analytical solution is that the former can be used to distinguish the above two different effects on the debonding loads.

The experimental and FE results have demonstrated that the debonding loads of the CFRP-to-steel interface are significantly reduced at both low and high service temperatures. This observation raises an important issue: the temperature effects need to be appropriately considered in practical strengthening design. However, the design guidance on how to consider the temperature effects is lacking in current design guidelines. Therefore, more research is needed to account for the temperature effects on the bond behavior and the associated debonding loads of CFRP-strengthened flexural steel members under different service temperature conditions.

## Acknowledgments

The authors would like to acknowledge the financial support supplied by the Nature Science Foundation of China (51978398 and 51478406), the Research Grants Council of the Hong Kong SAR (15219919) and the Natural Science Foundation of Shanghai (19ZR1426200).

## References

[1] Yu T, Fernando D, Teng JG, Zhao XL. Experimental study on CFRP-to-steel bonded interfaces. Composites Part B: Engineering, 2012; 43(5): 2279–2289.

[2] Teng JG, Yu T, Fernando D. Strengthening of steel structures with fiber-reinforced polymer composites. Journal of Constructional Steel Research, 2012; 78: 131–143.

[3] Zhao XL, Zhang L. State-of-the-art review on FRP strengthened steel structures. Engineering Structures, 2007; 29(8): 1808–1823.

[4] Gholami M, Sam ARM, Yatim JM, Tahir MM. A review on steel/CFRP strengthening systems focusing environmental performance. Construction and Building Materials, 2013; 47: 301–310.

[5] Sahin MU, Dawood M. Experimental investigation of bond between high-modulus CFRP and steel at moderately elevated temperatures. Journal of Composites for Construction, 2016; 20: 04016049.

[6] Nguyen T, Bai Y, Al-Mahaidi R, Zhao X. Time-dependent behavior of steel/CFRP double strap joints subjected to combined thermal and mechanical loading. Composite Structures, 2012; 94(5): 1834–1845.

[7] Stratford TJ, Bisby LA. Effect of warm temperatures on externally bonded FRP strengthening. Journal of Composites for Construction, 2012; 16(3): 235–244.

[8] Dai JG, Gao WY, Teng JG. Bond-slip model for FRP laminates externally bonded to concrete at elevated temperature. Journal of Composites for Construction, 2013; 17(2): 217–228.

[9] Green MF, Bisby LA, Fam AZ, Kodur VKR. FRP confined concrete columns: Behaviour under extreme conditions. Cement and Concrete Composites, 2006; 28(10): 928–937.

[10] Yoshitake I, Tsuda H, Itose J, Hisabe N. Effect of discrepancy in thermal expansion coefficients of CFRP and steel under cold temperature, Construction and Building Materials, 2014: 59: 17-24.

[11] Ke L, Li C, He J, Dong S, Chen C, Jiao Y. Effects of elevated temperatures on mechanical behavior of epoxy adhesives and CFRP-steel hybrid joints. Composite Structures, 2020; 235: 111789.

[12] Heshmati M, Haghani R, Al-Emrani M. Environmental durability of adhesively bonded FRP/steel joints in civil engineering applications: State of the art. Composites Part B: Engineering, 2015; 81: 259–275.

[13] Gao WY, Teng JG, Dai JG. Effect of temperature variation on the full-range behavior of FRP-to-concrete bonded joints. Journal of Composites for Construction, 2012; 16: 671–683.

[14] Gao WY, Dai JG, Teng JG. Analysis of Mode II debonding behavior of fiber-reinforced polymer-to-substrate bonded joints subjected to combined thermal and mechanical loading. Engineering Fracture Mechanics, 2015; 136: 241–264.

[15] Biscaia HC. The influence of temperature variations on adhesively bonded structures: A non-linear theoretical perspective. International Journal of Non-Liner Mechanics, 2019; 113: 67–85.

[16] Guo D, Gao WY, Fernando D, Dai JG. Effect of temperature variation on the plate-end debonding of FRP-strengthened beams: A theoretical study. Advances in Structural Engineering, 2022; 25: 290–305.

[17] Guo D, Gao WY, Dai JG. Effects of temperature variation on intermediate crack-induced debonding and stress intensity factor in FRP-retrofitted cracked steel beams: An analytical study. Composite Structures, 2022; 279: 114776.

[18] Guo D, Zhou H, Wang HP, Dai JG. Effect of temperature variation on the plate-end debonding of FRP-strengthened steel beams: coupled mixed-mode cohesive zone modeling, Engineering Fracture Mechanics, 2022; 108583.

[19] Zhou H, Gao WY, Biscaia HC, Wei XJ, Dai JG. Debonding analysis of FRP-to-concrete interfaces between two adjacent cracks in plated beams under temperature variations. Engineering Fracture Mechanics, 2022; 263: 108307.

[20] Dong K, Hu K. Development of bond strength model for CFRP-to-concrete joints at high temperatures. Composites Part B: Engineering, 2016; 95: 264–271.

[21] Zhou H, Torres JP, Fernando D, Law A, Emberley R. The bond behaviour of CFRP-to-steel bonded joints with varying bond properties at elevated temperatures. Engineering Structures, 2019; 183: 1121–1133.

[22] Jia DG, Gao WY, Duan DX, Yang J, Dai JG. Full-range behavior of FRP-to-concrete bonded joints subjected to combined effects of loading and temperature variation. Engineering Fracture Mechanics, 2021; 254: 107928.

[23] Liu HB, Zhao XL, Bai Y, Singh RK, Rizkalla S, Bandyopadhyay S. The effect of elevated temperature on the bond between high modulus carbon fibre-reinforced polymer sheet and steel. Australian Journal of Structural Engineering, 2014; 15: 355–366.

[24] Nguyen T, Bai Y, Zhao X, Al-Mahaidi R. Mechanical characterization of steel/CFRP double strap joints at elevated temperatures. Composite Structures, 2011; 93(6): 1604–1612.

[25] Al-Shawaf A, Al-Mahaidi R, Zhao X-L. Effect of elevated temperature on bond behaviour of high modulus CFRP/steel double-strap joints. Australian Journal of Structural Engineering, 2009; 10: 63–74.

[26] He J, Xian G, Zhang YX. Effect of moderately elevated temperatures on bond behaviour of CFRP-to-steel bonded joints using different adhesives. Construction and Building Materials, 2020; 241: 118057.

[27] Li S, Zhu T, Lu Y, Li X. Effect of temperature variation on bond characteristics between CFRP and steel plate. International Journal of Polymer Science, 2016; 5674572.

[28] Chandrathilaka E, Gamage J, Fawzia S. Mechanical characterization of CFRP/steel bond cured and tested at elevated temperature. Composite Structures, 2019; 207: 471–477.

[29] Zhou H, Fernando D, Torero JL, Torres JP, Maluk C, Emberley R. Bond behavior of CFRP-to-steel bonded joints at mild temperatures: Experimental study. Journal of Composites for Construction, 2020; 24: 04020070.

[30] Biscaia HC, Ribeiro P. A temperature-dependent bond-slip model for CFRP-to-steel joints. Composite Structures, 2019; 217: 186–205.

[31] Al-Shawaf AK. Characterization of bonding behavior between wet lay-up carbon fibre reinforced polymer and steel plates in double-strap joints under extreme environmental temperatures. Australia: Monash University, 2010.

[32] Al-Shawaf A, Zhao XL. Adhesive rheology impact on wet lay-up CFRP/steel joints' behaviour under infrastructural subzero exposures. Composites Part B: Engineering, 2013; 47: 207–219.

[33] Zhang Y, Vassilopoulos AP, Keller T. Effects of low and high temperatures on tensile behavior of adhesively-bonded GFRP joints. Composite Structures, 2010; 92: 1631–1639.

[34] Di Tommaso A, Neubauer U, Pantuso A, Rostasy FS. Behavior of adhesively bonded concrete-CFRP joints at low and high temperatures. Mechanics of Composite Materials, 2001; 37: 327–338.

[35] Park YB, Song MG, Kim JJ, Kweon JH, Choi JH. Strength of carbon/epoxy composite single-lap bonded joints in various environmental conditions. Composite Structures, 2010; 92: 2173–2180.

[36] Yao MX, Zhu DJ, Yao YM, Zhang HA, Mobasher B. Experimental study on basalt FRP/steel single-lap joints under different loading rates and temperatures. Composite Structures, 2016; 145: 68–79.

[37] ASTM D3039. Standard test method for tensile properties of polymer matrix composite materials. West Conshohocken, Philadelphia (PA): ASTM International; 2014.

[38] ASTM A370. Standard test methods and definitions for mechanical testing of steel products. West Conshohocken, Philadelphia (PA): ASTM International; 2014.

[39] ISO 11359-2. Plastics-thermomechanical analysis (TMA). Part 2: Determination of coefficient of linear thermal expansion and glass transition temperature. International Organization for Standardization: Geneva, Switzerland, 1999.

[40] ASTM D7028. Standard Test Method for Glass Transition Temperature (DMA Tg) of Polymer Matrix Composites by Dynamic Mechanical Analysis (DMA). West Conshohocken, Philadelphia (PA): ASTM International; 2007.

[41] Gao WY, Dai JG, Teng JG. Three-level fire resistance design of FRP-strengthened RC beams. Journal of Composites for Construction, 2018; 22(3): 05018001.

[42] Maluk C, Bisby LA, Terrasi G, Green MF. Bond strength of CFRP and steel bars in concrete at elevated temperature. ACI SP 279, American Concrete Institute, Farmington Hills, MI, 2011; 41–75.

[43] Fernando D, Teng JG, Yu T, Zhao XL. Preparation and characterization of steel surfaces for adhesive bonding. Journal of Composites for Construction, 2013;17(6): 04013012.

[44] Amada S, Satoh A. Fractal analysis of surfaces roughened by grit blasting. Journal of Adhesion Science and Technology, 2000;14(1): 27–41.

[45] Deng J, Lee MMK. Behaviour under static loading of metallic beams reinforced with a bonded CFRP plate. Composite Structures, 2007; 78: 232–242.

[46] Zeng JJ, Gao WY, Liu F. Interfacial behavior and debonding failures of full-scale CFRP-strengthened H-section steel beams. Composite Structures, 2018; 201: 540–552.

[47] Colombi P, Fava G, Sonzogni L. Fatigue crack growth in CFRP-strengthened steel plates. Composites Part B: Engineering, 2015; 72: 87–96.

[48] ACI 440.2R-08. Guide for the design and construction of externally bonded FRP systems for strengthening concrete structures, ACI Committee 440. Farmington Hills, MI, USA: American Concrete Institute; 2008.

[49] Concrete Society. Design guidance for strengthening concrete structures using fibre composite materials, Technical Report No. 55, 3rd edition, Camberley, UK, 2012.

[50] Barris C, Correia L, Sena-Cruz J. Experimental study on the bond behaviour of a transversely compressed mechanical anchorage system for externally bonded reinforcement. Composite Structures, 2018; 200: 217–228.

[51] Ko H, Matthys S, Palmieri A, Sato Y. Development of a simplified bond stress–slip model for bonded FRP-concrete interfaces. Construction and Building Materials, 2014; 68: 142–157.

[52] Yang Y, Biscaia H, Chastre C, Silva M. Bond characteristics of CFRP-to-steel joints. Journal of Constructional Steel Research, 2017; 138: 401–419.